Supporting Information

Ducros et al. 10.1073/pnas.1307818110

SI Text 1

Encoded Multisite Two-Photon Microscopy Encoding with *S* Matrices. We use the notation from ref. 1 that was developed in the framework of optical multiplexing for spectroscopic applications.

The codes used for encoded multisite two-photon microscopy (eMS2PM) are derived from Hadamard matrices, whose elements are +1 and −1 and characterized by the property

$$H_n \times H_n^T = n \cdot I_n, \qquad \text{[S1]}$$

where "×" is the matrix multiplication, $H_n{}^T$ is the transpose of matrix H_n, n is a power of 2, and I_n is the identity matrix of dimension n. In other words rows and columns are mutually orthogonal.

Hadamard matrices of order 2^k can be constructed as

$$H_1 = 1 \qquad \text{[S2]}$$

$$H_2 = \begin{bmatrix} 1 & 1 \\ 1 & - \end{bmatrix}, \qquad \text{[S3]}$$

where "−" stands for "−1", and

$$H_{2^k} = \begin{bmatrix} H_{2^{k-1}} & H_{2^{k-1}} \\ H_{2^{k-1}} & -H_{2^{k-1}} \end{bmatrix}. \qquad \text{[S4]}$$

For example, $H_8 =$

$$\begin{bmatrix} 1 & 1 & 1 & 1 & 1 & 1 & 1 & 1 \\ 1 & - & 1 & - & 1 & - & 1 & - \\ 1 & 1 & - & - & 1 & 1 & - & - \\ 1 & - & - & 1 & 1 & - & - & 1 \\ 1 & 1 & 1 & 1 & - & - & - & - \\ 1 & - & 1 & - & - & 1 & - & 1 \\ 1 & 1 & - & - & - & - & 1 & 1 \\ 1 & - & - & 1 & - & 1 & 1 & - \end{bmatrix}.$$

We call G_{n-1} H_n matrices without first row and columns

$$H_n = \begin{bmatrix} 1 & 1 \\ 1 & G_{n-1} \end{bmatrix}. \qquad \text{[S5]}$$

For example, $G_7 =$

$$\begin{bmatrix} - & 1 & - & 1 & - & 1 & - \\ 1 & - & - & 1 & 1 & - & - \\ - & - & 1 & 1 & - & - & 1 \\ 1 & 1 & 1 & - & - & - & - \\ - & 1 & - & - & 1 & - & 1 \\ 1 & - & - & - & - & 1 & 1 \\ - & - & 1 & - & 1 & 1 & - \end{bmatrix}.$$

Note that all rows and columns of G_{n-1} matrices have $n/2$ "−1" and $n/2-1$ "+1".

Because negative light modulation cannot be achieved, we replace −1 by 1 and 1 by 0 and define S_{n-1},

$$S_{n-1} = \frac{1}{2} \cdot (-G_{n-1} + J_{n-1}), \qquad \text{[S6]}$$

where J_{n-1} is a square matrix of dimension $n-1$ where all elements are 1.

For example, $S_7 =$

$$\begin{bmatrix} 1 & 0 & 1 & 0 & 1 & 0 & 1 \\ 0 & 1 & 1 & 0 & 0 & 1 & 1 \\ 1 & 1 & 0 & 0 & 1 & 1 & 0 \\ 0 & 0 & 0 & 1 & 1 & 1 & 1 \\ 1 & 0 & 1 & 1 & 0 & 1 & 0 \\ 0 & 1 & 1 & 1 & 1 & 0 & 0 \\ 1 & 1 & 0 & 1 & 0 & 0 & 1 \end{bmatrix}.$$

Codes used in eMS2PM correspond to the rows of matrix S, where 1 and 0 represent ON and OFF illumination states, respectively. Practically, encoding is achieved by applying a sequence of ON and OFF states to the digital micromirror devices (DMDs) that lie on the optical path of each user-defined region of interest (ROI).

The signal measured at the detector during the time of an S code is the sum of fluorescent signals from all targets that the can be expressed as a vector D,

$$D = [a_1 \ \ldots \ a_{n-1}] \times S_{n-1}, \qquad \text{[S7]}$$

where a_1 to a_{n-1} are the average fluorescence signals collected from targets 1 to $n-1$, which are assumed to be constant over the duration of an S code. Decoding the signals from each target consists in solving (Eq. **S7**) a system of $n-1$ linear equations with $n-1$ unknown. We can show from Eqs. **S4**–**S6** that

$$S_{n-1} \times \left(-G_{n-1}^T\right) = \mathrm{S_{n-1}} \times \mathrm{S_{n-1}^*} = \frac{n}{2} \cdot I_{n-1}. \qquad \text{[S8]}$$

Here we defined the decoding matrice $S_{n-1}{}^* = -\mathrm{G}_{n-1}{}^T$. Note that $S_{n-1}{}^*$ is identical to S_{n-1} except 0 is replaced by −1. Hence, decoding is simply computing the vector B: $[b_1 \ldots b_{n-1}]$ defined by $B = D \times S_{n-1}^*$:

$$B = [a_1 \ \ldots \ a_{n-1}] \times S_{n-1} \times S_{n-1}^* = \frac{n}{2} \cdot [a_1 \ \ldots \ a_{n-1}]. \qquad \text{[S9]}$$

Thus, the amplitude a_i originating from target i can be recovered by multiplying the sequence D measured at the detector by a decoding sequence, which is the ith column of matrix $S_{n-1}{}^*$.

For example, if the signals amplitude at targets 1–7 is [1 3 5 7 2 4 6], we have

$$\underbrace{[1\ \ 3\ \ 5\ \ 7\ \ 2\ \ 4\ \ 6]}_{\text{Amplitudes at targets : } [a_1 \ldots a_7]} \times \underbrace{\begin{bmatrix} 1 & 0 & 1 & 0 & 1 & 0 & 1 \\ 0 & 1 & 1 & 0 & 0 & 1 & 1 \\ 1 & 1 & 0 & 0 & 1 & 1 & 0 \\ 0 & 0 & 0 & 1 & 1 & 1 & 1 \\ 1 & 0 & 1 & 1 & 0 & 1 & 0 \\ 0 & 1 & 1 & 1 & 1 & 0 & 0 \\ 1 & 1 & 0 & 1 & 0 & 0 & 1 \end{bmatrix}}_{\text{Encoding matrix : } S_7} \times \underbrace{\begin{bmatrix} 1 & - & 1 & - & 1 & - & 1 \\ - & 1 & 1 & - & - & 1 & 1 \\ 1 & 1 & - & - & 1 & 1 & - \\ - & - & - & 1 & 1 & 1 & 1 \\ 1 & - & 1 & 1 & - & 1 & - \\ - & 1 & 1 & 1 & 1 & - & - \\ 1 & 1 & - & 1 & - & - & 1 \end{bmatrix}}_{\text{Decoding matrix : } S_7^* = -G_7^T} = \underbrace{[14\ \ 18\ \ 10\ \ 19\ \ 17\ \ 17\ \ 17]}_{\substack{\text{Sequence recorded at} \\ \text{detector : } D=[a_1 \ldots a_7] \times S_7}}$$

$$\times \underbrace{\begin{bmatrix} 1 & - & 1 & - & 1 & - & 1 \\ - & 1 & 1 & - & - & 1 & 1 \\ 1 & 1 & - & - & 1 & 1 & - \\ - & - & - & 1 & 1 & 1 & 1 \\ 1 & - & 1 & 1 & - & 1 & - \\ - & 1 & 1 & 1 & 1 & - & - \\ 1 & 1 & - & 1 & - & - & 1 \end{bmatrix}}_{\text{Decoding matrix : } S_7^* = -G_7^T} = \underbrace{4 \times [1\ \ 3\ \ 5\ \ 7\ \ 2\ \ 4\ \ 6]}_{4 \times\ [a_1 \ldots a_7]}.$$

For 2 or 3 ROIs, encoding follows the three-digit sequences given by rows of S_3 and decoding is achieved with S_3*. For 4–7 targets we use S_7 and S_7*, for 8–11 targets we use S_{11} and S_{11}*, and for 12–15 targets we use S_{15} and S_{15}*, . . . , etc. Matrices S_n and S_n* for $n = 3$, 7, 11, and 15 are displayed in Table S1.

In practice we have added a 0 (OFF) at the beginning of each S code. During this bin all excitation subbeams are turned off. Signal measured during this bin is subtracted from all other bins to remove offset due to background optical and electronic noises. Furthermore this black bin is used to precisely register acquired data with respect to the DMD frame clock, which is critical for perfect decoding. Thus, the codes used in the present work are $N + 1$ digits long for encoding up to N ROIs' signals.

The maximum refresh rate of the DMD (set to 16.6 kHz in the present setup) determines the shortest time for the ON or OFF states, i.e., the duration of each digit in the S codes. Therefore, a 7-digit S code lasts at least 8*60 μs = 0.48 ms, i.e., the shortest time resolution. For a 15-digit-long S code the time resolution is 0.96 ms minimum. The maximum DMD frame rate is 22.7 kHz for binary patterns according to manufacturer specifications. However, we found that for frame rates higher than ∼16 kHz, the light reflectance decreased significantly. This is likely due to the micromirrors settling time of ∼10 μs between each frame, during which light is not reflected into the setup. DMD with faster update rates and shorter settling times would permit lower eMS2PM time resolution.

SI Text 2

Theoretical Noise Performance of eMS2PM and Comparison with Sequential Scanning Method. Here we derive an equation for the signal-to-noise ratio (SNR) of the eMS2PM signals and compare it with the SNR that would be obtained with a sequential scan with the same time resolution, such as what is typically achieved by acousto-optic deflector (AOD)-based random access microscopy. We assume shot noise limited detection in both cases.

SNR with eMS2PM. $s_{i,j}$ is a set of M S codes of length N ($i = 1. . .M$, and $j = 1...N$). M is the number of ROIs. N is the number of bins in the S codes. The maximum value for M is N. $s_{i,j}$ are the rows of the S matrix defined in Table S1. Sequences $s_{i,j}$ modulate M subbeams that are focused onto spatially separated ROIs R_i. Each ROI R_i can be a single point, clusters of points, or any user-defined shapes.

$s^*_{i,j}$ is the set of decoding sequences associated with $s_{i,j}$ such that

$$\sum_{j=1}^{N} s_{i,j} \cdot s^*_{j,k} = \frac{N+1}{2} \delta_{i,k}, \qquad \textbf{[S10]}$$

where $\delta_{i,k} = 1$ if i = k and $\delta_{i,k} = 0$ if $i \neq k$.

We call a_{ij} the number of fluorescence photons emitted by ROI i during bin j of the S code. a_{ij} is proportional to τ, the duration of each binary state (ON or OFF). We assume that fluorescence signals from each ROI do not vary over the duration of an S code and that the random variations of $a_{i,j}$ are due to shot noise. Thus, $a_{i,j}$ can be written as the sum of a time-independent mean photon count $\overline{a_i}$ and a fluctuation $\varepsilon_{i,j}$:

$$a_{i,j} = \overline{a_i} + \varepsilon_{i,j}. \qquad \textbf{[S11]}$$

Furthermore for each ROI i, the variance of the photon count measured over a time bin (σ^2_{ai}) is equal the mean photon count ($\overline{a_i}$):

$$\sigma^2_{ai} = \overline{a_i}. \qquad \textbf{[S12]}$$

The signal d_j recorded at the detector during bin j of the S code is

$$d_j = \gamma \cdot \sum_{i=1}^{M} a_{i,j} \cdot s_{i,j} + \delta_j. \qquad \textbf{[S13]}$$

γ is a proportionality factor that takes into account collection efficiency and detector quantum yield and δ_j is an additional detection noise (thermal electronic noise, background optical noise) independent of detected fluorescence. In the following equations we assume $\gamma = 1$ for simplicity. Because $a_{i,\,j}$ are uncorrelated, the variance of d_j is then

$$\sigma^2_{dj} = \sum_{i=1}^{M} \overline{a_i} \cdot s^2_{i,j} + \sigma^2_{\delta}. \qquad \textbf{[S14]}$$

By definition the decoded signals are

$$b_k = \sum_{j=1}^{N} d_j \cdot s^*_{k,j} \qquad \textbf{[S15a]}$$

$$b_k = \sum_{j=1}^{N}\sum_{i=1}^{M} a_{i,j} \cdot s_{i,j} \cdot s^*_{k,j} + \sum_{j=1}^{N} \delta_j \cdot s^*_{k,j}. \qquad \textbf{[S15b]}$$

The average decoded signals are then

$$\overline{b_k} = \sum_{j=1}^{N} \overline{a_i} \cdot \sum_{i=1}^{M} s_{i,j} \cdot s^*_{k,j}. \qquad \textbf{[S16]}$$

Here the nonzero average detection noise is canceled by subtracting the average signal in the initial OFF bin applied before S code (*SI Text 1* and Fig. S1).

Finally, according to Eq. **S10**,

$$\overline{b_k} = \frac{N+1}{2} \cdot \overline{a_k}. \qquad \textbf{[S17]}$$

Because the d_j are uncorrelated, the variance of decoded signals b_k is, according to Eq. **S15a**,

$$\sigma^2_{bk} = \sum_{j=1}^{N} \sigma^2_{dj} \cdot s^{*2}_{i,j}. \qquad \textbf{[S18]}$$

From [**S14**]

$$\sigma^2_{bk} = \sum_{j=1}^{N}\sum_{i=1}^{M} \overline{a_i} \cdot s^2_{i,j} \cdot s^{*2}_{k,j} + \sum_{j=1}^{N} \sigma^2_{\delta} \cdot s^{*2}_{i,j} \qquad \textbf{[S19a]}$$

$$\sigma^2_{bk} = \sum_{i=1}^{M} \overline{a_i} \cdot \sum_{j=1}^{N} s^2_{i,j} \cdot s^{*2}_{k,j} + \sigma^2_{\delta} \cdot \sum_{j=1}^{N} s^{*2}_{i,j}. \qquad \textbf{[S19b]}$$

Because a column of $s_{i,j}$ matrices is composed of $(N + 1)/2$ "+1" and $(N - 1)/2$ "0", and $s^{*2}{}_{k,j} = +1$ for all k and j,

$$\sigma^2_{bk} = \frac{N+1}{2} \cdot \sum_{i=1}^{M} \overline{a_i} + N \cdot \sigma^2_{\delta}. \qquad \textbf{[S20]}$$

Assuming that the detection noise is negligible compared with the shot noise, we can derive the following equation for the decoded signal's SNR:

$$SNR_k = \frac{\sqrt{N+1}}{\sqrt{2}} \cdot \frac{\overline{a_k}}{\sqrt{\sum_{i=1}^{M} \overline{a_i}}}. \qquad \textbf{[S21]}$$

For example, if all ROIs emit the same average fluorescence signal $\bar{a}$, their SNR is

$$SNR = \frac{\sqrt{N+1}}{\sqrt{2}} \cdot \frac{\sqrt{\bar{a}}}{\sqrt{M}}. \qquad \textbf{[S22]}$$

The SNR decreases with the number of ROIs. This rule is further confirmed by the results displayed in Fig. S2.

Contrary to the classical single-point shot noise limited detection scheme, the SNR of decoded signals is not proportional to the square root of the mean photon count. It is smaller by a factor $1/\sqrt{M}$. This comes from the fact that the noise from all ROIs is summed together onto the detector before decoding.

SNR with sequential scanning method. Let us define $\bar{f}_{\text{seq}}$, the average photon flux emitted by a cellular fluorophore excited by a single point. If the laser remains δt on this point, $\overline{a}_{seq}$ photons are detected:

$$\overline{a}_{seq} = \delta t \cdot \bar{f}_{seq}. \qquad \textbf{[S23]}$$

As above for eMS2PM we considered that the proportionality factor γ that takes into account light collection efficiency and detector quantum yield is 1. For shot-noise limited detection the SNR is

$$SNR_{seq} = \sqrt{\overline{a}_{seq}} = \sqrt{\delta t \cdot \bar{f}_{seq}}. \qquad \textbf{[S24]}$$

If the laser is scanned between M points, the time resolution is

$$T = M \cdot \delta t. \qquad \textbf{[S25]}$$

We neglected the scanning time between each point. This situation is similar to AOD-based random access two-photon microscopy (2PM).

Comparison of eMS2PM and sequential scanning. Let us set an identical time resolution, T, for both methods:

$$T = M \cdot \delta t = N \cdot \tau. \qquad \textbf{[S26]}$$

So, if $M = N$,

$$\delta t = \tau. \qquad \textbf{[S27]}$$

And the eMS2PM SNR is

$$SNR = \frac{\sqrt{N+1}}{\sqrt{2}} \cdot \frac{\sqrt{\delta t \cdot \bar{f}}}{\sqrt{N}}, \qquad \textbf{[S28]}$$

where $\bar{f}$ is the mean photon flux emitted by a single ROI in eMS2PM mode. Then

$$\frac{SNR}{SNR_{seq}} = \frac{\sqrt{N+1}}{\sqrt{2N}} \frac{\sqrt{\bar{f}}}{\sqrt{\bar{f}_{seq}}}. \qquad \textbf{[S29]}$$

If $\bar{f} = \bar{f}_{seq}$, the eMS2PM approach yields a smaller SNR than sequential scanning approach by a factor $\sim 1/\sqrt{2}$. However, if the signal generated at each ROI is at least twice as high as the photon flux $\bar{f}_{seq}$, then the SNR in eMS2PM mode is greater than in sequential mode.

Note that $\bar{f}_{seq}$ is limited to a value $\bar{f}_{max}$ (between 10^5 and 10^7 photons per second at the detector, depending on the fluorophore concentration and the two-photon cross-section) that can be generated by a focused spot at maximum intensity below either phototoxicity or photobleaching. On the other hand, the photon flux $\bar{f}$ generated by any ROI in eMS2PM mode is not limited to $\bar{f}_{max}$. Multiple foci, each emitting fluorescence below $\bar{f}_{max}$, can be grouped in the same eMS2PM target (i.e., modulated with the same S codes) and are summed into the same decoded signal, thus increasing the SNR by $\sqrt{n_f}$, n_f being the number of foci.

The 2PM photobleaching rate is proportional to the third or fourth power of the intensity (2, 3). Thus, illuminating each ROI with multiple foci and reducing the intensity in each focus can drastically reduce photobleaching without loss of SNR. If laser power is sufficient, SNR can even be increased. For example, if we compare situation A, where N cells are targeted with one diffraction-limited spot of power P each, and situation B, where

the same cells are targeted with an ROI made of four diffracted limited spots of power $P/2$ each, the ROI SNRs are identical in both situations, whereas the photobleaching rate in all foci is reduced by a factor 1/8. The accumulated bleaching per ROI is two times smaller in case B than in case A. However, case B requires twice as much laser power as case A.

SI Methods

Setup Light Transmission. Spatial light modulator (SLM) diffraction efficiency was around 90%. The DMD, which is an array of 1,024 × 768 micromirrors (13 μm × 13 μm), diffracted light into multiple orders, among which a single one was collected by the effective NA of subsequent optics. We precisely oriented the angle of incidence in 3D to maximize the efficiency of diffraction into the collected order to 45%. Power transmission/reflection by all other optical elements (all dielectric mirrors, $R \sim 95\%$; all lenses, $T \sim 90\%$; dichroic mirrors DIC1 and DIC 2, $T \sim 90\%$; objective 63×, $T \sim 65\%$) represented a reduction of ∼50%. Thus, the maximum available power at the sample was around 500 mW. In HEK cells experiments we used ∼5 mW per ROI (∼1 mW per point). In acute slice experiments (Fig. 4) and in vivo (Fig. 5), at depth >200 μm, we used between 40 and 100 mW per ROI (measured at the surface).

SLM and DMD Damage Threshold. SLM maximum peak power is 50 GW·cm^{-2} for 50-fs pulses at 1 kHz repetition rate (2.7 W average). We remained in a more favorable case with 0.6 GW·cm^{-2} for 70-fs pulses at 80 MHz (average power 2.6 W). The damage threshold for the DMD matrix is around 0.1 J·cm^{-2} per pulse for nanosecond pulses, as specified by the manufacturer, but no information is available for shorter pulses. We remained below 10^{-4} J·cm^{-2}.

2PM and eMS2PM Optical Setups Coalignment. The 2PM and eMS2PM image planes had to be precisely coaligned in 3D to ensure that targets drawn onto 2PM images were precisely illuminated and modulated by the eMS2PM setup. A thin fluorescent layer (<1 μm thick, rhodamine B in plastic) was placed at the objective focal plane and fluorescence patterns excited either by the 2PM or by the eMS2PM setup were acquired by a CCD camera (not drawn on Fig. 1). Initially, the 2PM and eMS2PM optical axis and focal planes were manually coaligned by fine opto-mechanical positioning of optical elements. To ensure precise overlapping of both image planes we added a Fresnel lens to the SLM hologram. Then, we used a semiautomatic procedure to compute the spatial affine transformation matrix M_{SLM} between the 2PM and the eMS2PM image coordinate systems:

1) Nine reference points (3 × 3 array, 100 μm side) are successively focused onto the rhodamine sheet with the 2PM. These nine diffraction-limited fluorescent points are imaged onto the CCD camera and their positions $(x_i, y_i)^{2PM}$ $i = 1...9$ are recorded.

2) A virtual image with the nine reference points is transformed into eMS2PM coordinates by multiplication by the affine matrix M_{SLM}. The resulting image is the input intensity profile of the iterative Fourier-transform (ifta) algorithm that computes the SLM phase profile (4, 5). The nine fluorescent spots created by eMS2PM are imaged onto the CCD and their positions are recorded: $(x_i, y_i)^{eMS2PM}$.

3) The mean distance d between the reference points $(x_i, y_i)^{2PM}$ and the targeted points $(x_i, y_i)^{eMS2PM}$ is computed.

Steps *2* and *3* are repeated for various M_{SLM} coefficients. The optimization consists in finding the best M_{SLM} that minimizes d. The optimization process is stopped for $d < 0.5$ μm. During this part of the alignment procedure the DMD pixels stay always ON.

Finally a secondary affine transformation matrix M_{DMD} that translates DMD pixels into sample coordinates is computed with the same type of optimization method. M_{DMD} is required to apply ROI-specific modulations patterns.

Aberration Correction for Fluorescence Intensity Optimization. We corrected static setup aberrations by adding a phase-correction mask to the SLM profile. To compute the correction mask we placed a fluorescent layer at the objective focal plane. The focal spot intensity was automatically maximized by an optimization algorithm that adjusted the amplitude of Zernicke terms for astigmatism, coma, and spherical aberrations.

Data Processing. Fluorescence traces from DiO-labeled HEK cells were acquired at 0.48-ms time resolution and not filtered. $\Delta F/F$ traces in Fig. 4 *A* and *B* were acquired at 2-ms time resolution and in Fig. 4*C* at 4-ms time resolution. All Fig. 4 traces are filtered at 20 Hz with a second-order Butterworth filter in LabVIEW. Time resolution was 2 ms for traces in Fig. 5*A*, as well as for traces 1–4 in Fig. 5*B*, and 1 ms for traces 5–7 in Fig. 5*B*. All plots in Fig. 5 were processed with a 17-point moving average filter in Clampfit. (PCLAMP; Molecular Devices). Images in Fig. 5 *A* and *B* were average projection of five images (2-μm step between successive images) ±4 μm above and below the plane where the eMS2PM ROIs were placed. The time resolution of the 12 traces recorded in blood vessels (Fig. 5*C*) was 0.96 ms. Fig. 5*C* traces were not filtered.

In Vivo Experimental Procedures. All animal care and experimentation was performed in accordance with the Institut National de la Santé et de la Recherche Médicale Animal Care and Use Committee guidelines. During surgery mice (C57BL/6; $n = 4$ for calcium imaging experiments and $n = 3$ for blood flow imaging experiments) were anesthetized with ketamine and xylazine (i.p. bolus of 90 mg/kg body weight and 10 mg/kg body weight, respectively). An ∼4-mm diameter craniotomy was performed about 2.5 mm posterior and 2 mm lateral from Bregma. The dura matter was removed and a drop of agarose gel [2.5% (wt/vol)] poured onto the brain. Anesthesia was maintained with isofluorane (0.5–1%) during the rest of the experiment. Animal breathing frequency was continuously monitored through a pneumogram transducer (BIOPAC Systems). The animal's temperature was monitored with a rectal thermometer and maintained at 37 °C with a feedback-controlled heating blanket (Harvard Apparatus). The method for electroporating cortical neurons was similar to the protocol in ref. 6: We used OGB1 hexapotassium salt (1 mM; Invitrogen) diluted in PBS, with 2-Hz, −50-V, 24-ms, 50-s pulse trains. For blood flow imaging experiments (Fig. 5*C*) we labeled plasma by i.v. injection of 200 μL of 150 kDa fluorescein dextran (0.5 mM; Sigma-Aldrich). Fluorescence transients due to red blood cell passage could be reliably recorded with eMS2PM down to 350 μm in all animals.

1. Harwit M, Sloane NJA (1979) *Hadamard Transform Optics* (Academic, New York).
2. Chen TS, Zeng SQ, Luo QM, Zhang ZH, Zhou W (2002) High-order photobleaching of green fluorescent protein inside live cells in two-photon excitation microscopy. *Biochem Biophys Res Commun* 291(5):1272–1275.
3. Patterson GH, Piston DW (2000) Photobleaching in two-photon excitation microscopy. *Biophys J* 78(4):2159–2162.
4. Papagiakoumou E, de Sars V, Oron D, Emiliani V (2008) Patterned two-photon illumination by spatiotemporal shaping of ultrashort pulses. *Opt Express* 16(26):22039–22047.
5. Lutz C, et al. (2008) Holographic photolysis of caged neurotransmitters. *Nat Methods* 5 (9):821–827.
6. Nagayama S, et al. (2007) In vivo simultaneous tracing and Ca(2+) imaging of local neuronal circuits. *Neuron* 53(6):789–803.

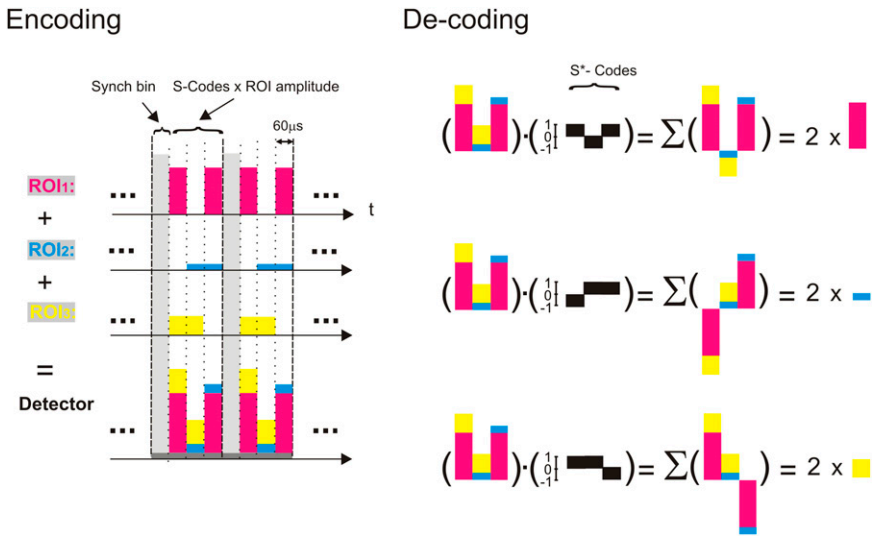

Fig. S1. Encoding and decoding steps with S codes for three ROIs. In the encoding phase, each ROI is excited by a different sequence composed of four 60-µs-long ON or OFF bins. Sequences are played repeatedly by the DMD. The initial synchronization bin (gray columns) that is always OFF is required to measure and subtract background noise, whereas the next three bins are the S codes. ROIs 1, 2, and 3 are excited with the S codes (1,0,1), (0,1,1), and (1,1,0), respectively. The amplitude of fluorescence emissions, which are ROI specific and modulated by the excitation patterns, adds up onto the detector, with an additional background noise (dark gray horizontal band). In the decoding phase, the background-corrected signal recorded at the detector during the three S-code bins is multiplied by ROI-specific decoding S* codes: (1,−1,1), (−1,1,1), and (1,1,−1) for ROIs 1, 2, and 3, respectively. The results are proportional to each ROI fluorescence amplitude.

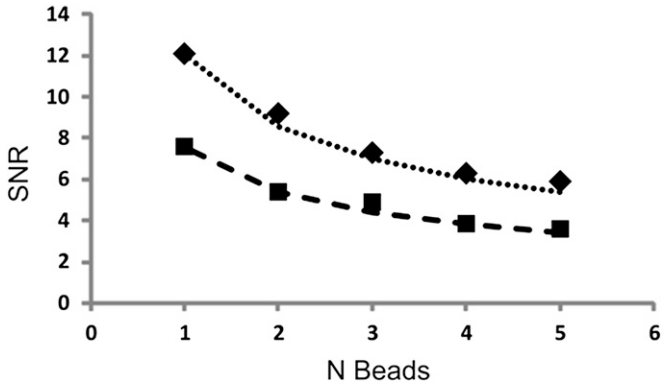

Fig. S2. The SNR of decoded fluorescent signals decreases as a function of the square root of the total detected power. A sample containing calibrated fluorescent beads (4 µm diameter, TetraSpeck; Molecular Probes) was imaged with the 2PM. We targeted between 1 and 5 beads (*N* Beads) with near diffraction-limited points and recorded the eMS2PM signals during 1 s with a time resolution of 0.48 ms. The excitation power in all points was identical. As expected from a shot-noise limited detection scheme the SNR of the decoded eMS2PM signals decreased as $1/\sqrt{N\ Beads}$ (solid squares, fitted by dashed line). In other words, the SNR was inversely proportional to the square root of the total detected power. The same experiment was reproduced with a time resolution of 0.96 ms (solid diamonds). The SNR of decoded signals, which was ~1.4 times greater than with a 0.48-ms time resolution for any number of imaged beads, decreased as $1/\sqrt{N\ Beads}$ (dotted line). This experiment confirmed the theoretical prediction of *SI Text 2*, and the observations of Fig. 2, that the noise in each individual decoded trace is the shot noise due to the sum of signals from all ROIs.

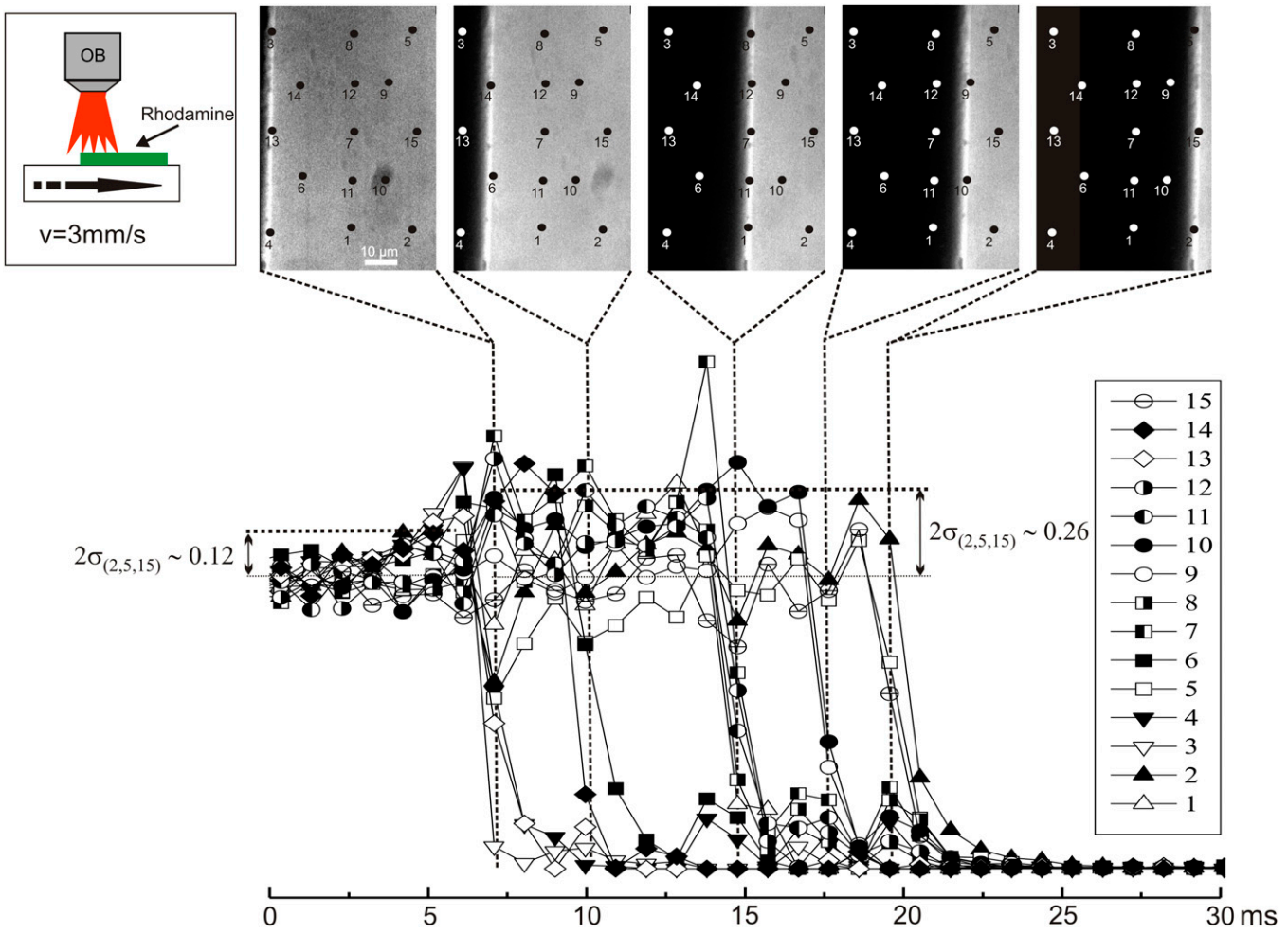

Fig. S3. Recording fluorescent transients in 15 sites with eMS2PM at submillisecond time resolution. A thin fluorescent sheet (Rhodamine in plastic, ~1 μm thick) with a sharp straight boundary was translated from left to right at 3 mm·s^{-1} (*Inset*, *Upper Left*). Fifteen points were manually placed in a region of about 50 μm × 75 μm in five groups aligned in columns parallel to the boundary. From left to right, the columns included the randomly selected points (4, 13, 3), (6, 14), (1, 11, 7, 12, 8), (10, 9), and (2, 15, 5). Each point *i* was encoded according to the *i*th S code, i.e., the *i*th line of the *S* matrix shown in Table S1. An S code lasted 0.96 ms. Excitation power per point was ~5 mW. Initially all points were inside the fluorescent sample (*Left*). Then, as the sample was translated to the right, the five columns of points reach the boundary one after the other. The decoded signals are normalized to their baseline value (0–5 ms). eMS2PM was able to precisely detect fast fluorescent transients occurring either simultaneously (e.g., points 1, 11, 7, 12, and 6 at t = 15 ms) or with delays in the order of a few milliseconds (e.g., 2-ms delay between ON/OFF transitions for points 10 and 15). This performance was independent of the index of the S codes that were randomly ordered, further demonstrating that fluorescence signals were truly sampled simultaneously—and not successively—in all 15 points. The signal fluctuation (displayed as twice the average SD, $2 \times \sigma_{2,5,15}$ of traces 2, 5, and 15, for clarity reasons) approximately doubled between the baseline (0–5 ms) and the transition period (8–20 ms). This is due in part to the effect of the very fast transients that induce small decoding artifacts and to the nonhomogenous rhodamine concentration near the edge. Here we demonstrated that eMS2PM could record fluorescence signals simultaneously in up to 15 sites at 0.96-ms time resolution.

Table S1. Coding and decoding matrices for 2–15 ROIs

N ROIs	Coding matrix	Decoding matrix	*T*, ms
2–3	$\begin{bmatrix}1&0&1\\0&1&1\\1&1&0\end{bmatrix}$	$\begin{bmatrix}1&-&1\\-&1&1\\1&1&-\end{bmatrix}$	0.24
4–7	$\begin{bmatrix}1&0&1&0&1&0&1\\0&1&1&0&0&1&1\\1&1&0&0&1&1&0\\0&0&0&1&1&1&1\\1&0&1&1&0&1&0\\0&1&1&1&1&0&0\\1&1&0&1&0&0&1\end{bmatrix}$	$\begin{bmatrix}1&-&1&-&1&-&1\\-&1&1&-&-&1&1\\1&1&-&-&1&1&-\\-&-&-&1&1&1&1\\1&-&1&1&-&1&-\\-&1&1&1&1&-&-\\1&1&-&1&-&-&1\end{bmatrix}$	0.48
8–11	$\begin{bmatrix}1&1&0&1&1&1&0&0&0&1&0\\1&0&1&1&1&0&0&0&1&0&1\\0&1&1&1&0&0&0&1&0&1&1\\1&1&1&0&0&0&1&0&1&1&0\\1&1&0&0&0&1&0&1&1&0&1\\1&0&0&0&1&0&1&1&0&1&1\\0&0&0&1&0&1&1&0&1&1&1\\0&0&1&0&1&1&0&1&1&1&0\\0&1&0&1&1&0&1&1&1&0&0\\1&0&1&1&0&1&1&1&0&0&0\\0&1&1&0&1&1&1&0&0&0&1\end{bmatrix}$	$\begin{bmatrix}1&1&-&1&1&1&-&-&-&1&-\\1&-&1&1&1&-&-&-&1&-&1\\-&1&1&1&-&-&-&1&-&1&1\\1&1&1&-&-&-&1&-&1&1&-\\1&1&-&-&-&1&-&1&1&-&1\\1&-&-&-&1&-&1&1&-&1&1\\-&-&-&1&-&1&1&-&1&1&1\\-&-&1&-&1&1&-&1&1&1&-\\-&1&-&1&1&-&1&1&1&-&-\\1&-&1&1&-&1&1&1&-&-&-\\-&1&1&-&1&1&1&-&-&-&1\end{bmatrix}$	0.72
12–15	$\begin{bmatrix}0&0&0&1&0&0&1&1&0&1&0&1&1&1&1\\0&0&1&0&0&1&1&0&1&0&1&1&1&1&0\\0&1&0&0&1&1&0&1&0&1&1&1&1&0&0\\1&0&0&1&1&0&1&0&1&1&1&1&0&0&0\\0&0&1&1&0&1&0&1&1&1&1&0&0&0&1\\0&1&1&0&1&0&1&1&1&1&0&0&0&1&0\\1&1&0&1&0&1&1&1&1&0&0&0&1&0&0\\1&0&1&0&1&1&1&1&0&0&0&1&0&0&1\\0&1&0&1&1&1&0&0&0&1&0&0&1&1&1\\1&0&1&1&1&1&0&0&0&1&0&0&1&1&0\\0&1&1&1&1&0&0&0&1&0&0&1&1&0&1\\1&1&1&1&0&0&0&0&0&0&1&1&0&1&0\\1&1&1&0&0&0&0&0&0&1&1&0&1&0&1\\1&1&0&0&0&0&0&0&1&1&0&1&0&1&1\\1&0&0&0&0&0&0&1&1&0&1&0&1&1&1\end{bmatrix}$	$\begin{bmatrix}-&-&-&1&-&-&1&1&-&1&-&1&1&1&1\\-&-&1&-&-&1&1&-&1&-&1&1&1&1&-\\-&1&-&-&1&1&-&1&-&1&1&1&1&-&-\\1&-&-&1&1&-&1&-&1&1&1&1&-&-&-\\-&-&1&1&-&1&-&1&1&1&1&-&-&-&1\\-&1&1&-&1&-&1&1&1&1&-&-&-&1&-\\1&1&-&1&-&1&1&1&1&-&-&-&1&-&-\\1&-&1&-&1&1&1&1&-&-&-&1&-&-&1\\-&1&-&1&1&1&1&-&-&-&1&-&-&1&1\\1&-&1&1&1&1&-&-&-&1&-&-&1&1&-\\-&1&1&1&1&-&-&-&1&-&-&1&1&-&1\\1&1&1&1&-&-&-&-&-&-&1&1&-&1&-\\1&1&1&-&-&-&-&-&-&1&1&-&1&-&1\\1&1&-&-&-&-&-&-&1&1&-&1&-&1&1\\1&-&-&-&-&-&-&1&1&-&1&-&1&1&1\end{bmatrix}$	0.96

S_n matrices for $n = 3$ and 7 were constructed from Hadamard matrices (*SI Text 1*). S_n matrices $n = 11$ and 15 are cyclic *S* matrices from ref. 1. For $n > 15$ see appendix A2 of ref. 1. The corresponding temporal resolutions (*T*) are indicated in the right column.